Journal of Applied Physics ARTICLE pubs.aip.org/aip/jap

Key parameters to optimize the photothermoelectric effect of thermoelectric materials

Cite as: J. Appl. Phys. **136**, 073103 (2024); doi: 10.1063/5.0219048
Submitted: 14 May 2024 · Accepted: 31 July 2024 ·
Published Online: 15 August 2024

Cheng-Hao Yin,[1,2] Hong-Tao Jiang,[1,2] Li-Da Chen,[1,3] Yang-Yang Lv,[1,3] Shu-Hua Yao,[1,3,4,a)] Jian Zhou,[1,3] Y. B. Chen,[1,2,b)] Ming-Hui Lu,[1,3,5] and Yan-Feng Chen[1,3,5]

AFFILIATIONS

[1]National Laboratory of Solid State Microstructures, Nanjing University, Nanjing 210093, China
[2]Department of Physics, Nanjing University, Nanjing 210093, China
[3]Jiangsu Key Laboratory of Artificial Functional Materials and Department of Materials Science and Engineering, Nanjing University, Nanjing 210093, China
[4]Hubei Key Laboratory of Plasma Chemistry and Advanced Materials, Wuhan Institute of Technology, Wuhan 430205, China
[5]Collaborative Innovation Center of Advanced Microstructures, Nanjing University, Nanjing 210093, China

[a)]**Author to whom correspondence should be addressed:** shyao@nju.edu.cn
[b)]**Email:** ybchen@nju.edu.cn

ABSTRACT

Recently, photothermoelectric effect of thermoelectric materials has been hotly explored to develop self-powered and large bandwidth photodetectors working at ambient conditions. However, the key parameters for optimized photothermoelectric effect are still elusive. Here, based on the two-temperature model under static condition, we theoretically studied the key parameters to optimize the photothermoelectric performance of thermoelectric materials. Results verify that when the incident electromagnetic wave only generates electronic intra-band excitation, there is an ideal carrier concentration to optimize the photothermoelectric voltage; when the wavelength of a detected electromagnetic wave can resonantly excite quasi-particle (like phonons) except electrons, the photothermoelectric voltage can be enhanced significantly around the resonant wavelength regime; and when the electronic inter-band transition can be excited by an electromagnetic wave, photothermoelectric voltage is significantly increased due to the high optical absorption. As an example, the theoretical dependence of the photothermoelectric voltage of SnSe on wavelength is in line with the experimental result. This work elucidates the crucial parameters of thermoelectric materials to achieve the ideal photothermoelectric performance.

I. INTRODUCTION

Recently, photothermoelectric effect (PTE) has been hotly explored for photo-detection because of ultra-broadband response and free-of-cooling unit.[1] In physics, PTE includes photothermal and thermoelectric conversion processes. In the photothermal process, materials absorb the energy of electromagnetic waves and generate local high temperatures and corresponding temperature gradients.[2,3] In the thermoelectric conversion process, electrical carriers are driven by temperature differences. Temperature difference can be generated by either hot electrons or hot phonons, which are nominated as hot-electron PTE and hot-phonon PTE in this work, respectively. As many works reported, graphene is one of the typical hot-electron PTE candidates.[4–6] The theoretical work, based on the two-temperature model under transient condition, has verified that the key parameters of hot-electron PTE are geometric parameters of the PTE devices, size of the light spot, and the electric mobility of materials.[7–10] Compared to hot-electron PTE, hot-phonon PTE study is mainly focused on thermoelectric materials, such as doped Si, Bi_2Se_3, $SrTiO_3$, $EuBiSe_3$, and SnSe, taking advantage of their large Seebeck coefficient

(>300 μV/K).[11–17] These materials have exhibited the significant PTE. However, these works are mainly focused on experimental characterizations rather than theoretical ones. In addition, in contrast to the rich theoretical studies of hot-electron PTE, there are a few theoretical works of hot-phonon PTE. In principle, there are some different features between hot-phonon PTE and hot-electron PTE, including the following (i) the hot-phonon PTE is a quasi-static process rather than the transient one[18] and (ii) temperature difference (ΔT) is mainly generated by hot phonons rather than hot electrons. These cases have not been systematically studied previously.

Taking the above-mentioned backgrounds into account, here, we theoretically studied the effects of physical parameters of an imaginary doped semiconductor (to simulate the thermoelectric materials[19]) on PTE voltage by using the two-temperature model under static condition. Optical processes between electromagnetic waves and thermoelectric materials in hot-phonon PTE include electronic intra-band, quasi-particle resonance, and electronic inter-band excitations.

II. THEORETICAL MODELS OF PTE AND CALCULATION RESULTS

Before the presentation of detailed calculations, we would like to outline the structure of this paper for easy understanding. Slow PTE includes photothermal and thermoelectric processes. The photothermal process is simulated by a modified two-temperature model, as shown in Sec. II A. As to describe the interaction between materials and electromagnetic waves, we use two classic models (Drude and Lorentz models) to describe the electronic intra-band excitation and quasi-particle resonance excitation, respectively, discussed in Sec. II B. It should be mentioned that quasi-particle resonance excitations include electronic inter-band excitation, as well as quasi-particle excitations except for quasi-electrons (such as phonons). The PTE voltage ΔU can be calculated by the Seebeck coefficient S of a doped semiconductor and the temperature difference ΔT ($\Delta U = -S \times \Delta T$).

A. Modified two-temperature model

In this part, we first calculated ΔT between two ends of the material under electromagnetic-wave irradiation by using the modified two-temperature model, so as to obtain the PTE voltage through $\Delta U = -S \times \Delta T$. The two-temperature model is a theoretical model to describe the evolution of hot-electron temperature (T_e) and hot-phonon temperature (T_i) of materials under the irradiation of incident electromagnetic waves. In the two-temperature model,[20,21] the evolution of T_e and T_i can be written as

$$\begin{cases} c_e \dfrac{\partial T_e}{\partial t} = -g(T_e - T_i) + I(t), \\ c_i \dfrac{\partial T_i}{\partial t} = g(T_e - T_i), \end{cases} \tag{1}$$

where c_e and c_i are heat capacities of electrons and phonons, respectively, and g is the electron-phonon-coupling constant. The incident electromagnetic wave is assumed as a Gaussian temporal profile,[22]

$$I(t) = (1 - R)\frac{2F_0}{\tau_L}\sqrt{\frac{\ln 2}{\pi}}\exp\left[-4\ln 2\left(\frac{t}{\tau_L}\right)^2\right], \tag{2}$$

where R is the reflectance, F_0 is the incident laser (electromagnetic-wave fluence), and τ_L is the laser pulse duration. Generally speaking, after a pulse of laser is incident on the sample, the electromagnetic-wave energy is first absorbed by the band electrons in a very short time ($\sim 10^{-15}$ s), and T_e rises rapidly accordingly.[18] Then, the extra energy of hot electrons is gradually transferred to phonons through electron-phonon-coupling at the time scale ($\sim 10^{-12}$ s).[18] With time, T_i rises but T_e decreases, and the material finally reaches the thermal equilibrium.

To simulate the general PTE experiments, the model is modified because many researchers use continuous-wave lasers to characterize the PTE properties of thermoelectric materials.[1,11] Accordingly, the equations of the modified two-temperature model are

$$\begin{cases} c_e \dfrac{\partial T_e}{\partial t} = -g(T_e - T_i) + (1 - R)\dfrac{I_0}{L_p}, \\ c_i \dfrac{\partial T_i}{\partial t} = g(T_e - T_i) - \alpha \Delta T, \end{cases} \tag{3}$$

where $I_0 = 0.5$ W/mm^2 is the averaged laser power exposed to samples and L_p is the penetration depth. α is a coefficient of heat dissipation with a form of $\alpha = \frac{\kappa}{L_c^2} = \frac{(C_V v_s)^2}{\kappa} = 1 \times 10^{12}$ W/(m^3 $\times$K), where κ is the thermal conductivity. L_c is considered as the thermal dissipation length which can be expressed by $L_c = \sqrt{\frac{\kappa}{\gamma_c C_V}}$,[10,23] where C_V is the thermal capacity, $\gamma_c = \frac{1}{\tau_c} = \frac{\bar{v}_{\text{sound}}}{l_{\text{phonon}}}$ is the cooling rate, and l_{phonon} is the mean-free-path of phonons.

In Eq. (3), first, we change the term of incident laser to a constant to simulate the continuous wave. Second, the system is considered to reach equilibrium in a short time due to the long-time scale (~micro-second) in the experiment because the absorbed laser energy is mainly dissipated by phonons. Therefore, we can approximate ΔT as the phonon temperature difference and set the temperature of the cold side as room temperature. We approximated the temperature distribution ($\nabla[\kappa \nabla T_i]$) of thermal transportation as $\alpha \Delta T$ because it is accurate enough, which is discussed in the supplementary material in detail. After reaching the thermal equilibrium, the time derivative terms of T_e and T_i in Eq. (3) are zero. Then, we can get

$$\Delta T = \frac{(1 - R)I_0}{\alpha L_p}. \tag{4}$$

Equation (4) is the fundamental formula of this paper. Using Eq. (4), we can get the dependence of ΔT on R and L_p in the subsequent parts. In Sec. II B, we will discuss the relationship between R and L_p and electromagnetic-wave frequency ω (wavelength $\lambda = \frac{2\pi c}{\omega}$,

where c is the light velocity) through the dielectric constants of materials to calculate ΔT.

B. Photothermoelectric voltage under different absorption conditions

The relationship of R and refractive index n is $R = \frac{(n-1)^2+k^2}{(n+1)^2+k^2}$.[24] The penetration process of laser beam in materials decays in the form of $e^{-2\pi kx/\lambda}$, so we can write $L_p = \frac{\lambda}{4\pi k}$ (k is the extinction coefficient).[24] In the following discussion, we will calculate the R and L_p in three optical processes of materials that are electronic intra-band excitation, quasi-particle (except electrons) excitation, and electronic inter-band excitation.

1. N and k in the case of electronic intra-band excitation

First, we calculate n and k of materials with ω in electronic intra-band absorption at low frequencies through the complex relative permittivity in the Drude model,[24]

$$\varepsilon_{\text{intra}} = (n+ik)^2 = 1 + i\frac{\sigma}{4\pi\varepsilon_0\omega}, \tag{5}$$

where $\sigma = \frac{Ne_0^2\tau}{m}$ is the electrical conductivity, N is the carrier concentration, e_0 is the charge of the electron, τ is the transport relaxation time which is set as 1×10^{-12} s most of the time in this paper, m is the effective mass of the carrier, and ε_0 is vacuum permittivity. It should be mentioned that in this paper, we assume that σ is only dependent on N, though N is correlated to τ. Using Eq. (5), we can get

$$\begin{cases} n_{\text{intra}} = \sqrt{\dfrac{1+\sqrt{1+\left(\dfrac{\sigma}{4\pi\varepsilon_0\omega}\right)^2}}{2}}, \\ k_{\text{intra}} = \sqrt{\dfrac{-1+\sqrt{1+\left(\dfrac{\sigma}{4\pi\varepsilon_0\omega}\right)^2}}{2}}. \end{cases} \tag{6}$$

2. n and k in the case of quasi-particle resonance excitation

When the wavelength of the electromagnetic wave is increased but still lower than the electronic bandgap, it is possible to generate other quasi-particle excitations (a type of resonance excitation), for example, phonons and magnons in magnetic materials.[25] Macroscopically, these types of quasi-particle excitations can be described by the Lorentz function.[24] In mathematics, the real part and imaginary part of ε can be written as

$$\begin{cases} \varepsilon'_{res} = 1 + \dfrac{N_r e_0^2}{\varepsilon_0 m}\dfrac{\omega_0^2-\omega^2}{(\omega_0^2-\omega^2)^2+\gamma^2\omega^2}, \\ \varepsilon''_{res} = \dfrac{e_0^2\tau}{4\pi\varepsilon_0\omega m}N + \dfrac{N_r e_0^2}{\varepsilon_0 m}\dfrac{\gamma\omega}{(\omega_0^2-\omega^2)^2+\gamma^2\omega^2}, \end{cases} \tag{7}$$

where N_r is the concentration of the quasi-particle set as 1×10^{21} cm^{-3} in this work; $\omega_0 = 7.60\times10^{14}$ (corresponding wavelength $\lambda_0 = 2480$ nm) is the resonant frequency; and γ is the full-width-at-half-maximum (FWHM) which is set as 1×10^{14} normally in this paper without specification. Thus, the expressions of n and k can be written as

$$\begin{cases} n_{res} = \sqrt{\dfrac{\varepsilon'_{res} + \sqrt{\varepsilon'^2_{res} + \left(\dfrac{e_0^2}{\varepsilon_0 m}\right)^2\left(\dfrac{\tau}{4\pi\omega}N + \dfrac{N_r\gamma\omega}{(\omega_0^2-\omega^2)^2+\gamma^2\omega^2}\right)^2}}{2}}, \\ k_{res} = \sqrt{\dfrac{-\varepsilon'_{res} + \sqrt{\varepsilon'^2_{res} + \left(\dfrac{e_0^2}{\varepsilon_0 m}\right)^2\left(\dfrac{\tau}{4\pi\omega}N + \dfrac{N_r\gamma\omega}{(\omega_0^2-\omega^2)^2+\gamma^2\omega^2}\right)^2}}{2}}. \end{cases} \tag{8}$$

3. N and k in the case of electronic inter-band excitation

When the energy of the electromagnetic wave is higher than the electronic bandgap, there are electronic inter-band transitions. In this case, the dielectric constants of materials are much more abstract than those in the intra-band and quasi-particle resonance excitation cases. In this part, we assume that there are three inter-transition bands of electrons, simulated by three Lorentz functions with large γ, when the energy of the electromagnetic wave is higher than the electronic bandgap. Then, ε becomes

$$\begin{cases} \varepsilon'_{\text{inter}} = 1 + \sum_{i=1}^{3}\dfrac{N_i e_0^2}{\varepsilon_0 m}\dfrac{\omega_i^2-\omega^2}{(\omega_i^2-\omega^2)^2+\gamma_i^2\omega^2}, \\ \varepsilon''_{\text{inter}} = \dfrac{e_0^2\tau}{4\pi\varepsilon_0\omega m}N + \sum_{i=1}^{3}\dfrac{N_i e_0^2}{\varepsilon_0 m}\dfrac{\gamma_i\omega}{(\omega_i^2-\omega^2)^2+\gamma_i^2\omega^2}. \end{cases} \tag{9}$$

We can get n and k from this complex dielectric constant and write them as n_0 and k_0. In addition, considering the electronic density-of-states around the bottom of the conduction band, we establish an absorption model as[24]

$$k_{\text{inter}} = k_0 + a\sqrt{E-E_0}, \tag{10}$$

where a is a parameter and E_0 is approximately equal to the bottom of the lowest conduction band. Using the Kramers–Kronig relations,[24] we can calculate $n_{\text{inter-band}}$ from $k_{\text{inter-band}}$.

Based on Eqs. (8)–(10), the n and k in the three cases (electronic intra-band, inter-band, and quasi-particle resonance excitations) are calculated and depicted in Fig. 1(a). When the wavelength of the incident electromagnetic wave is in the range of $1700-3200$ nm (low energy), we show that n and k consider both electronic intra-band and quasi-particle resonance absorption. Obviously, there is a peak (~2480 nm) in both n and k curves. Quantitatively, n and k change from 1–2 to 5–6 around the resonance regimes. While the wavelength is in the range of $400-1600$ nm (high energy), n and k also have several broad peaks corresponding

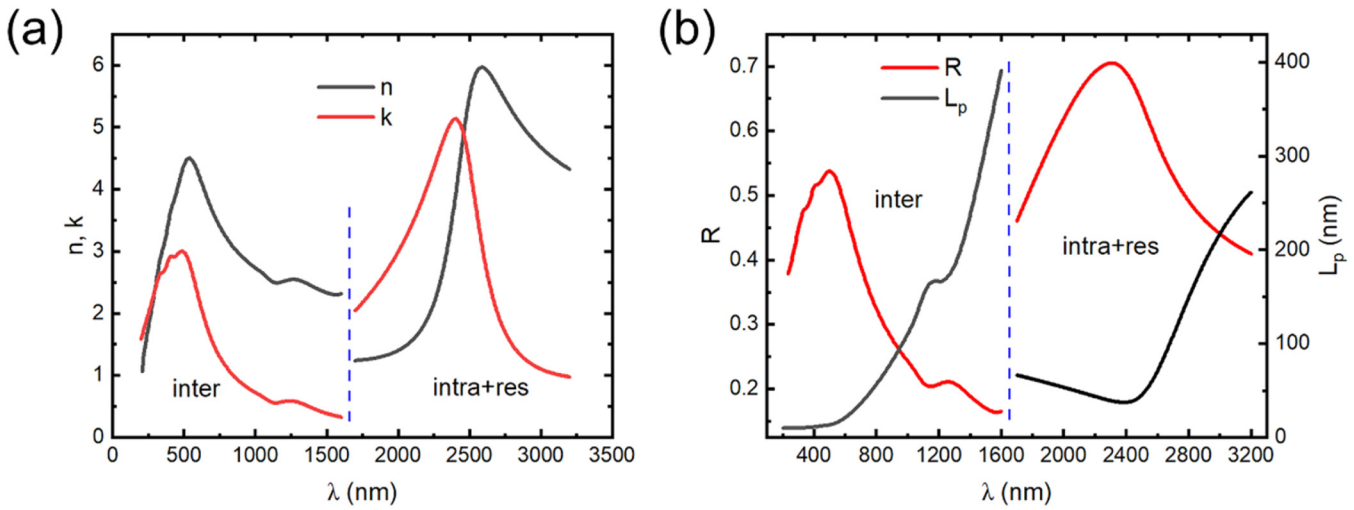

FIG. 1. (a) The dependence of refractive index n and optical extinction coefficient k of thermoelectric materials on the electromagnetic wavelength λ. The black and red lines represent n and k, where the left part (200–1600 nm) is considered as electronic inter-band absorption, while the right part (1700–3200 nm) comes from the electronic intra-band (Drude term), as well as quasi-particle (besides quasi-electron, for example, phonon) resonance absorption. The wavelength of quasi-particle resonance absorption is set as $\lambda_0 = 2480$ nm. (b) The dependence of reflectance R and penetration depth L_p of thermoelectric materials on the wavelength of incident laser based on n and k shown in (a).

to the electronic inter-band absorption. The positions of the three conduction bands are set at about $300 - 550$ nm, so n and k are higher at this regime too. According to n and k shown in Fig. 1(a), R and L_p can be calculated and depicted in Fig. 1(b). Evidently, R has the peak feature around resonance regimes and L_p decreases dramatically around resonance regimes. Quantitatively, L_p decreases from 260 to 40 nm when λ decreases from 3200 to 2480 nm.

4. ΔT and photothermoelectric voltage ΔU in different absorption cases

According to the above-mentioned n and k, we can get expressions of ΔT at three cases as Eqs. (11)–(13), respectively,

$$\Delta T_{\text{intra}} = \frac{I_0 e_0^2 \tau}{\pi \varepsilon_0 m c \alpha} \frac{N}{\sqrt{1+\left(\frac{e_0^2\tau}{4\pi\varepsilon_0\omega m}\right)^2 N^2} + 1 + \sqrt{2} \times \sqrt{1+\sqrt{1+\left(\frac{e_0^2\tau}{4\pi\varepsilon_0\omega m}\right)^2 N^2}}}, \tag{11}$$

$$\Delta T_{res} = \frac{4 I_0 \omega}{c\alpha} \frac{\varepsilon''_{res}}{|\varepsilon_{res}| + 1 + \sqrt{2} \times \sqrt{\varepsilon'_{res} + |\varepsilon_{res}|}}, \tag{12}$$

$$\Delta T_{\text{inter}} = \frac{(1 - R_{\text{inter-band}}) I_0}{\alpha L_{p,\text{inter-band}}}. \tag{13}$$

Taking advantage of Eqs. (11)–(13), the numerically calculated ΔT in the three cases are shown in Fig. 2. We can see that ΔT increased when N increased in all three cases. In the case of electronic intra-band absorption, the carrier concentration N in the Drude model has a prominent influence on the change in n and k, so the change of ΔT with N is the largest, which is about 0.4 K. However, in the quasi-particle resonance absorption case

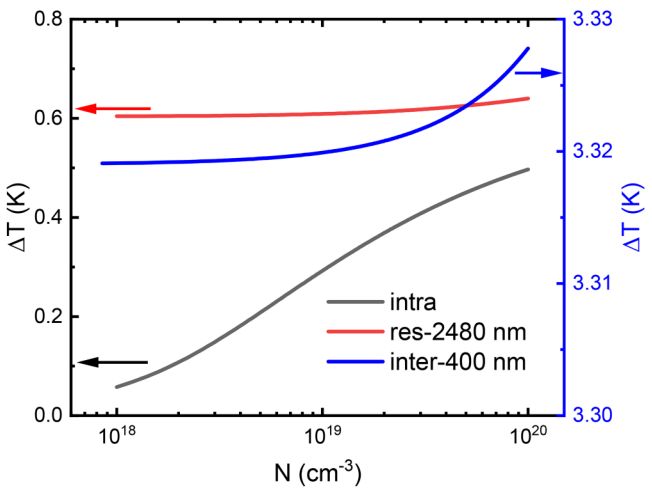

FIG. 2. The temperature difference ΔT of thermoelectric materials increases with the raising of carrier concentration N in all three cases: electronic intra-band, quasi-particle resonance, and electronic inter-band absorption. ΔT is significantly enhanced with increased N in the electronic intra-band absorption case (see the black line); while ΔT is slightly dependent on carrier concentration N in the cases of quasi-particle resonance and electronic inter-band absorption (see the red line and the blue line).

($\lambda = \lambda_0 = 2480$ nm) and the electronic inter-band case ($\lambda = 400$ nm), the Drude term is nearly negligible. As a result, ΔT in these two cases changes little with N, which are smaller than 0.05 K. In addition, contribution of the Drude term in the case of the electronic inter-band (400 nm) is smaller than that of quasi-particle resonance absorption (2480 nm), leading to that ΔT is nearly independent of N in the electronic inter-band case.

Generally speaking, thermoelectric materials belong to narrow-bandgap semiconductors.[19] Therefore, we used the Seebeck coefficient S of semiconductors to simulate that of the thermoelectric materials. Accordingly, S can be expressed as[19]

$$S = \frac{k_B}{e_0}\left(\frac{5}{2} - \ln\left(\frac{h^3}{2}(2\pi m k_B T)^{-\frac{3}{2}}N\right)\right), \tag{14}$$

where k_B is the Boltzmann constant and h is the Planck constant.

In the case of electronic intra-band absorption, we can get PTE voltage as

$$\Delta U_{\text{intra}} = \frac{e_0 k_B I_0 \tau}{\pi\varepsilon_0 mc\alpha} \frac{\left(\frac{5}{2} + \ln 2 - \frac{3}{2}\ln\left(\frac{h^2}{2\pi m k_B T}\right) - \ln N\right)N}{\sqrt{1 + \left(\frac{e_0^2\tau}{4\pi\varepsilon_0\omega m}\right)^2 N^2} + 1 + \sqrt{2} \times \sqrt{1 + \sqrt{1 + \left(\frac{e_0^2\tau}{4\pi\varepsilon_0\omega m}\right)^2 N^2}}}. \tag{15}$$

Using Eqs. (11), (14), and (15), we can calculate ΔT and S in the electronic intra-band case and depict the result in Fig. 3. Obviously, ΔT increases when N is raised, while S decreases simultaneously. As a result, there is a maximum value of ΔU in an optimized carrier concentration N_{opt} because of the trade-off between S and ΔT.

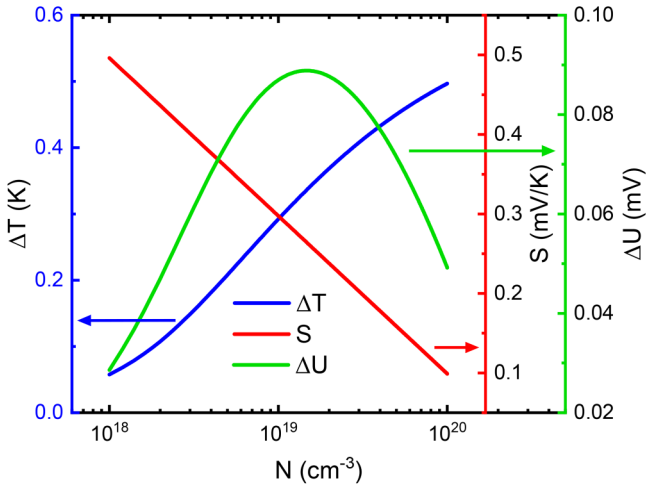

FIG. 3. In the case of electronic intra-band absorption, the Seebeck coefficient S of thermoelectric materials decreases with carrier concentration N raised (see the red curve). While the temperature difference ΔT that resulted from the photothermoelectric (PTE) effect increases with increased N (see the blue curve). Therefore, electric voltage ΔU due to the PTE effect shows a "dome-like" dependence on N (see the green curve).

Considering quasi-particle resonance absorption, the PTE voltage is

$$\Delta U_{res} = \frac{4k_B I_0 \omega}{e_0 c\alpha}\left(\frac{5}{2} - \ln\left(\frac{h^3}{2}(2\pi m k_B T)^{-\frac{3}{2}}N\right)\right)\frac{\varepsilon''_{res}}{|\varepsilon_{res}| + 1 + \sqrt{2} \times \sqrt{\varepsilon'_{res} + |\varepsilon_{res}|}}. \tag{16}$$

According to formula (16), we can see that ΔU depends on N, λ, and γ. In Fig. 4(a), we depict the numerical result of dependences of ΔU on N and λ as a 3D diagram. Evidently, ΔU is much larger when λ of the electromagnetic wave matches the resonant wavelength than other conditions. In order to clearly show the enhancement caused by quasi-particle resonance absorption, we compare the dependence of ΔU on N when λ is 2480, 2000, and 1800 nm, respectively, in Fig. 4(b). Obviously, ΔU (~0.3 mV) under the quasi-particle resonance absorption condition is larger than only the electronic intra-band absorption condition (~0.09 mV)at almost all wavelengths λ. In addition, different from the electronic intra-band absorption case, there is no extremum of ΔU with N changed around the resonant wavelength. Figure 4(c) shows the variation of ΔU with λ with different N ($N = 1$, 2, and 4×10^{19} cm^{-3}). One can see that the maximum of ΔU with λ is nearly located at the resonant wavelength (~2480 nm). Figure 4(d) demonstrates the effect of γ on the dependence of ΔU on N under $\lambda = 2480$ nm. Obviously, the smaller γ leads to a larger ΔU. Quantitatively, ΔU increases from about 0.075 to 0.2 mV when γ decreases from 1×10^{15} to 1×10^{13} Hz (N is set as 1×10^{19} cm^{-3} in calculation). Therefore, to have the largest ΔU, we should choose optical resonances with minimum γ.

In the electronic inter-band absorption case, the dependence of ΔU on N or λ is calculated and plotted as a 3D diagram in Fig. 5(a). To see Fig. 5(a) more clearly, we plot the dependence of ΔU on N under three specific wavelengths ($\lambda = 400$, 600, and 1000 nm) in Fig. 5(b). Evidently, ΔU decreases when N increases, no matter in any wavelength. The decrease in ΔU is mainly due to the decrease in S when N is increased. As a result, ΔT increases very slowly (see Fig. 2). In addition, shorter wavelength of electromagnetic waves leads to higher ΔU. Quantitatively, ΔU increases from about 0.1 to 0.6 mV when λ decreases from 1000 to 400 nm (N is set as 4×10^{19} cm^{-3}). Figure 5(c) is the relationship between ΔU and λ under three specific carrier concentrations N ($N \sim 1$, 2, and 4×10^{19} cm^{-3}). Obviously, ΔU decreases when λ increases, which is attributed to the smaller energy of electromagnetic waves to excite electronic inter-band transition inefficiently.

In summary, based on the above-mentioned calculations, we would like to discuss the insights for ideal thermoelectric materials to efficiently detect electromagnetic waves through hot-phonon PTE. First, it is ideal to use electronic inter-band absorption to maximize the PTE voltage. Therefore, choosing thermoelectric materials with suitable electronic bandgaps that match the measured electromagnetic-spectral range. Second, choosing thermoelectric materials with suitable resonance absorption to match the measured electromagnetic spectrum. Here, resonance absorption is either the intrinsic quasi-particle excitation (like phonons as

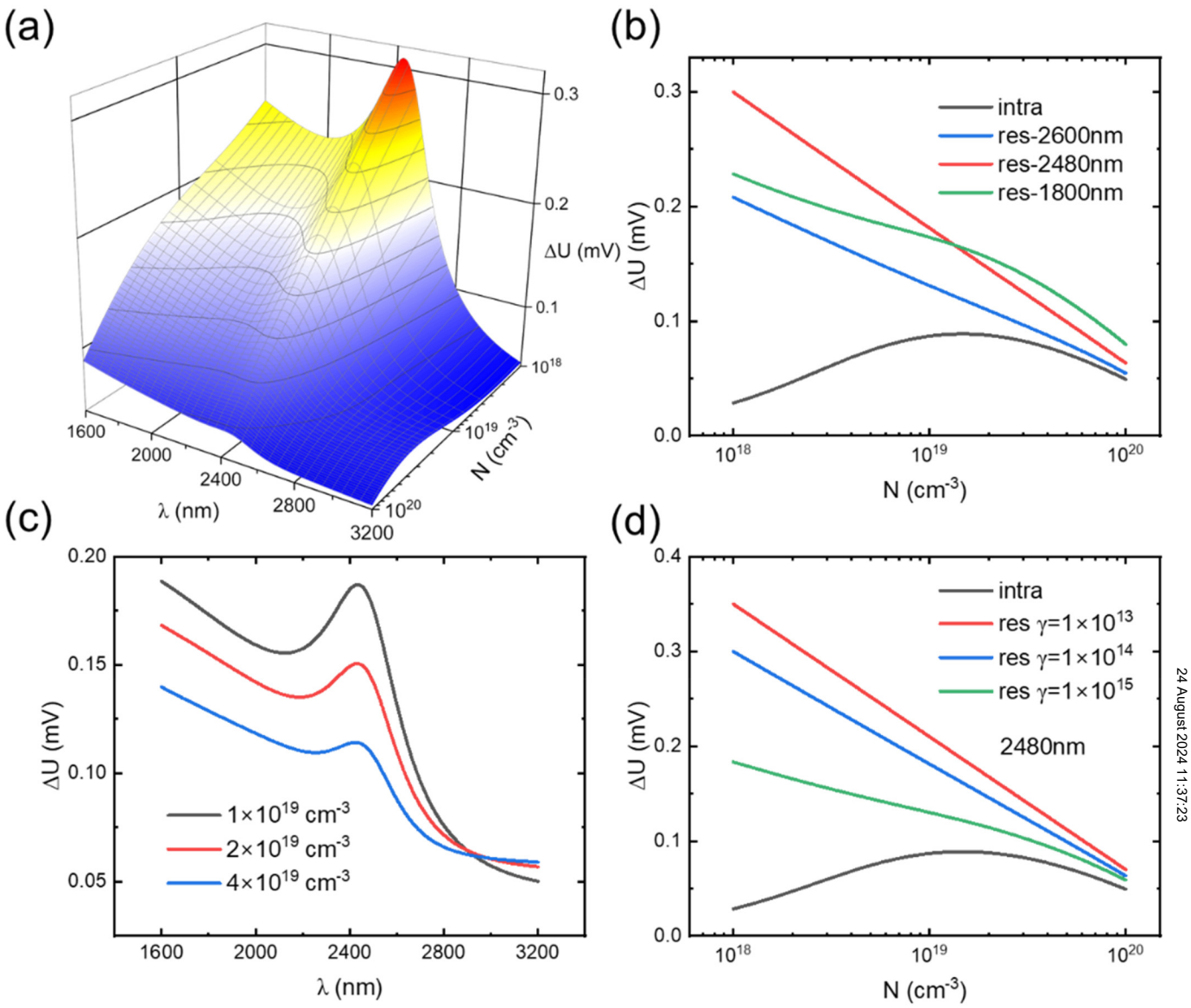

FIG. 4. (a) is the 3D diagram of the dependence of ΔU in thermoelectric materials with N and λ, under the conditions of both electronic intra-band and quasi-particle resonance absorptions. (b) The dependence of ΔU of thermoelectric materials on carrier concentration N under different electromagnetic wavelengths ($\lambda = 1800$, 2000, and 2480 nm). We can see that when $\lambda = 2480$ nm matches the resonant frequency, ΔU decreases monotonically with N. Besides, ΔU at the resonant wavelength is larger than the electronic intra-band absorption case, especially when N is lower than 4×10^{19} cm^{-3}. (c) shows the relationship between ΔU and λ with different N in electronic intra-band and quasi-particle resonance absorption cases ($N = 1$, 2, and 4×10^{19} cm^{-3}). One can see that ΔU has a maximum near the resonant wavelength. (d) is the dependence of ΔU on N at different full-width-at-half-maximum (FWHM) γ of resonance peaks ($\gamma = 1 \times 10^{13}$, 10^{14}, and 10^{15} Hz). Obviously, ΔU becomes larger with smaller γ. ΔU in the case of quasi-particle resonance is higher than that of the electronic intra-band case.

reported[11]) or man-made meta-structures (like Mie modes in spherical nano-meter particles[26]). Third, if we measure electromagnetic waves whose energy is smaller than those of electronic inter-band and resonance excitations, we should carefully process the thermoelectric materials to have an ideal carrier concentration to maximize the PTE (see Fig. 3).

III. COMPARISON WITH EXPERIMENTAL

We measured the PTE in SnSe crystals with different electron and hole concentrations previously.[17] Here, we applied the above-discussed theory to discuss the experimental results in detail. First, we measured the n and k of SnSe crystals through ellipsometry as

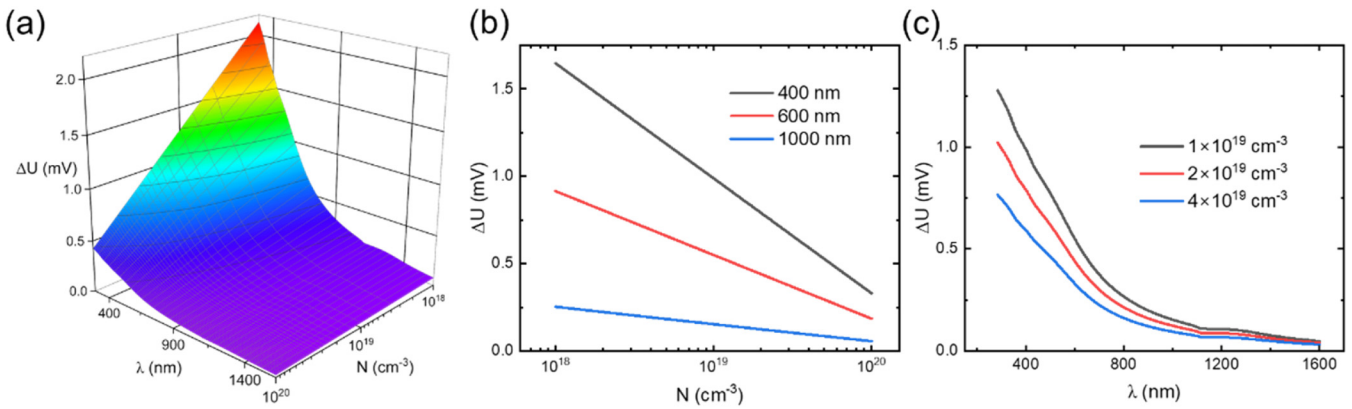

FIG. 5. (a) is the 3D diagram of the dependence of ΔU in thermoelectric materials on N and λ considering electronic inter-band absorption. (b) The dependence of ΔU on N under different wavelengths of electromagnetic waves ($\lambda = 400$, 600, and 1000 nm) in electronic inter-band absorption. (c) shows the dependence of ΔU on λ with different N ($N \sim 1$, 2, and 4×10^{19} cm^{-3}) in the electronic inter-band absorption case.

presented in Fig. 6(a). Compared with the theoretical n/k at the inter-band absorption region shown in Fig. 1(a), we can find that the experimental and the theoretical n is a little different in the long-wavelength region. This discrepancy comes from the theoretical n calculated by k using the Kramers–Kronig relations, which should integrate from minus to plus infinite frequency. However, the calculating range of n is much smaller than reality that we cannot get the n fitted to experimental ones. Although the experimental and the theoretical n seem different, they have quite similar absorption peaks which we can quantitatively analyze and compare their components in Fig. S1 in the supplementary material. It is found that the broadening feature of n at the long-wavelength region mainly comes from more optical transitions between valence and conduction bands in real compounds.

We used the experimental $n$and k of the SnSe crystal to calculate ΔT using Eq. (4) directly and depicted the results in Fig. 6(b). Two sets of experimental data with different electrical conductivities (σ equals 40 and 125 Ω^{-1}cm^{-1}) are shown in Fig. 6(b).

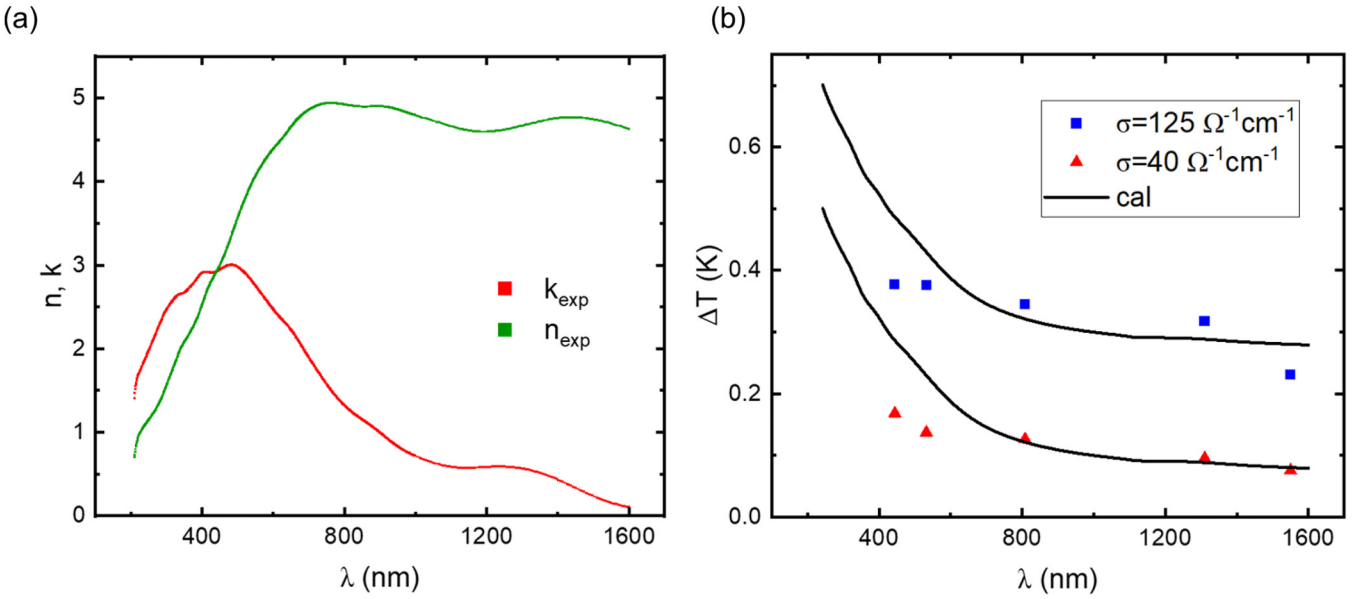

FIG. 6. (a) The green and red dots are experimental n and k of SnSe crystals measured by ellipsometry. (b) shows the comparison between experimental and theoretical ΔT of p-/n-type SnSe crystals under different wavelength electromagnetic-wave irradiation. The theoretical ΔT curves are calculated by Eq. (4) in the main text.

Evidently, the theoretical dependence of ΔT of SnSe crystals on λ is in line with the experimental data at the long-wavelength regime (800–1600 nm), but is poorly fit to experiment at the short-wavelength regime (400–600 nm). We attributed this discrepancy to the following problem. In experiments, the measured voltage and temperature differences are the values from the right and left electrodes, while the theoretical temperature difference is the value from the radiation point to the right electrode. Generally, the experimental temperature difference ΔT is always smaller than the theoretical one. We calculated the temperature distribution of one example using Comsol software, which is shown in Fig. S2 in the supplementary material. In accordance with this mechanism, we think that when ΔT is low, like in the long-wavelength range (800–1600 nm) of SnSe, temperature distribution at the radiation point is relatively flat and the temperature of the radiation point has little difference with the temperature of the left electrode. Thus, theoretical ΔT is quite close to the experimental one. However, in the case of inter-band electronic transition at the short-wavelength regime (400–600 nm) of SnSe, the temperature at the radiation point changes sharply and is significantly higher than that of the left electrode. Obviously, theoretical ΔT deviates much from the experimental value. Therefore, we believe that our photothermoelectric theory gives the upper-limit/maximum value of temperature difference due to the photothermoelectric effect.

IV. CONCLUSIONS

In closing, we use the modified two-temperature model to calculate the temperature difference and the resultant photothermoelectric voltage of thermoelectric materials under static conditions. These results verify that when the electromagnetic wave generates only the electronic intra-band excitation, there is an ideal electronic concentration to have the maximum photothermoelectric voltage, coming from the trade-off between the Seebeck coefficient and optical absorption. When the quasi-particle (except electrons) can be excited by electromagnetic waves, photothermoelectric voltage can be resonantly enhanced around the resonant wavelength regime. When the energy of the electromagnetic wave is high enough to generate the electronic inter-band excitation, photothermoelectric voltage is higher than those of the electronic intra-band and quasi-particle resonance excitation cases due to the high optical absorption in this case. Our theory can be applied to understand the experimental relationship between the photothermoelectric voltage of *n*-type/*p*-type SnSe crystals and the wavelength of electromagnetic waves. This work gives clear guidelines to choose suitable thermoelectric materials and engineer their electric properties to have the ideal photothermoelectric effect.

SUPPLEMENTARY MATERIAL

We put some supplementary information into the supplementary material for readers to refer to mentioned in the text, which includes (1) the derivation process of the term $\alpha\Delta T$ from $\nabla[\kappa\nabla T_i]$ in the modified two-temperature model, (2) the absorption peak analyses of experimental n and k compared with the theoretical ones, and (3) the analysis of the error between theoretical and experimental temperature differences with numerical simulation using Comsol.

ACKNOWLEDGMENTS

We wish to acknowledge the financial support from the Foundation for Innovative Research Groups of the National Natural Science Foundation of China (No. 51721001) and the National Natural Science Foundation of China (NNSFC) (Nos. 52331008, 52272002, 51902152, 11874210, 11974163, and 11890702).

AUTHOR DECLARATIONS

Conflict of Interest

The authors have no conflicts to disclose.

Author Contributions

Cheng-Hao Yin: Conceptualization (equal); Data curation (equal); Formal analysis (lead); Writing – original draft (lead); Writing – review & editing (equal). **Hong-Tao Jiang:** Conceptualization (supporting); Data curation (equal); Writing – review & editing (supporting). **Li-Da Chen:** Conceptualization (equal); Data curation (supporting); Writing – review & editing (supporting). **Yang-Yang Lv:** Methodology (supporting). **Shu-Hua Yao:** Methodology (equal); Supervision (lead); Writing – review & editing (equal). **Jian Zhou:** Supervision (supporting). **Y. B. Chen:** Methodology (equal); Supervision (lead); Writing – review & editing (equal). **Ming-Hui Lu:** Supervision (supporting). **Yan-Feng Chen:** Investigation (supporting); Methodology (supporting); Supervision (lead).

DATA AVAILABILITY

The data that support the findings of this study are available from the corresponding author upon reasonable request.

REFERENCES

[1]X. Lu, L. Sun, P. Jiang, and X. Bao, Adv. Mater. **31**, 1902044 (2019).
[2]N. M. Gabor, Z. Zhong, K. Bosnick, J. Park, and P. L. Mceuen, Science **325**, 1367 (2009).
[3]N. M. Gabor, J. C. W. Song, Q. Ma, N. L. Nair, T. Taychatanapat, K. Watanabe, T. Taniguchi, L. S. Levitov, and P. Jarillo-Herrero, Science **334**, 648 (2011).
[4]D. Sun, G. Aivazian, A. M. Jones, J. S. Ross, W. Yao, D. Cobden, and X. D. Xu, Nat. Nanotechnol. **7**, 114 (2012).
[5]K. J. Tielrooij, L. Piatkowski, M. Massicotte, A. Woessner, Q. Ma, Y. Lee, K. S. Myhro, C. N. Lau, P. Jarillo-Herrero, N. F. van Hulst, and F. H. L. Koppens, Nat. Nanotechnol. **10**, 437 (2015).
[6]K. J. Tielrooij, N. C. H. Hesp, A. Principi, M. B. Lundeberg, E. A. A. Pogna, L. Banszerus, Z. Mics, M. Massicotte, P. Schmidt, D. Davydovskaya, D. G. Purdie, I. Goykhman, G. Soavi, A. Lombardo, K. Watanabe, T. Taniguchi, M. Bonn, D. Turchinovich, C. Stampfer, A. C. Ferrari, G. Cerullo, M. Polini, and F. H. L. Koppens, Nat. Nanotechnol. **13**, 41 (2018).
[7]B. C. St-Antoine, D. Ménard, and R. Martel, Nano Lett. **9**, 3503 (2009).
[8]B. C. St-Antoine, D. Ménard, and R. Martel, Nano Res. **5**, 73 (2012).
[9]X. W. He, X. Wang, S. Nanot, K. Cong, Q. J. Jiang, A. A. Kane, J. E. M. Goldsmith, R. H. Hauge, F. Léonard, and J. Kono, ACS Nano **7**, 7271 (2013).
[10]A. Antidormi and A. W. Cummings, Phys. Rev. Appl. **15**, 054049 (2021).
[11]X. W. Lu, P. Jiang, and X. H. Bao, Nat. Commun. **10**, 138 (2019).
[12]W. Dai, W. Liu, J. Yang, C. Xu, A. Alabastri, C. Liu, P. Nordlander, Z. Guan, and H. Xu, Light Sci. Appl. **9**, 120 (2020).

[13]Y. Yan, Z.-M. Liao, X. Ke, G. Van Tendeloo, Q. Wang, D. Sun, W. Yao, S. Zhou, L. Zhang, H.-C. Wu, and D.-P. Yu, Nano Lett. **14**, 4389 (2014).
[14]K. W. Mauser, S. Kim, S. Mitrovic, D. Fleischman, R. Pala, K. C. Schwab, and H. A. Atwater, Nat. Nanotechnol. **12**, 770 (2017).
[15]Y. Wang, Y. Niu, M. Chen, J. Wen, W. Wu, Y. Jin, D. Wu, and Z. Zhao, ACS Photonics **6**, 895 (2019).
[16]W. Deng, C. Wang, M. Dai, F. Wang, J. Han, F. Sun, Q. J. Wang, and Y. Zhang, Appl. Phys. Lett. **121**, 112105 (2022).
[17]L.-D. Chen, H.-T. Jiang, C.-H. Yin, E.-R. Zhang, Y.-Y. Hou, X.-L. Zhou, F. Wang, Y.-Y. Lv, X.-J. Yan, J. Zhou, S.-H. Yao, Y. B. Chen, M.-H. Lu, and Y.-F. Chen, Appl. Phys. Lett. **123**, 041102 (2023).
[18]L.-X. Ye, *Semiconductor Physics* (Higher Education Press, Beijing, 2007).
[19]D. K. C. MacDonald and D. Tuomi, J. Electrochem. Soc. **110**, 206C (1963).
[20]S. Anisimov, B. L. Kapeliovich, and T. Perelman, Zh. Eksp. Teor. Fiz **66**, 375 (1974).
[21]T. Derrien, T. Sarnet, M. Sentis, and T. Itina, J. Optoelectron. Adv. Mater. **12**, 610 (2010).
[22]N. M. Bulgakova, R. Stoian, A. Rosenfeld, I. V. Hertel, W. Marine, and E. E. B. Campbell, Appl. Phys. A **81**, 345 (2005).
[23]J. C. W. Song, M. S. Rudner, C. M. Marcus, and L. S. Levitov, Nano Lett. **11**, 4688 (2011).
[24]M. Fox, *Optical Properties of Solids* (Oxford University Press, New York, 2010).
[25]C. Kittel, *Introduction to Solid State Physics* (Wiley, New York, 1986).
[26]E. N. Economou, *The Physics of Solids: Essentials and Beyond* (Springer-Verlag, Berlin, 2010).